Electronic Structure and Properties of Solids

Jeremy K. Burdett

Department of Chemistry and James Franck Institute, The University of Chicago, Chicago, Illinois 60637

Received: December 8, 1995; In Final Form: February 20, 1996⊗

Some of the challenges facing scientists in the area of the electronic structure and properties of solids are reviewed. At a time when computational advances have made possible high-quality calculations, not even conceivable 10 years ago, the article stresses the importance of going beyond the raw output of the calculation and understanding where the result originates. The areas selected for study include the Fermi surface and charge density waves, the stability of solids and the structures of solids under pressure, metal−insulator transitions, the method of moments, superconductivity, and the use of a relatively new technique for the study of chemical bonding, the electron localization function (ELF).

1. Introduction

Understanding the structures and physical properties of materials, such as hardness and the occurrence of metal−insulator transitions, has long been a goal of the chemist and materials scientist alike. Our understanding of the structures of molecules and solids has progressed dramatically in the past decade driven by computational advances in terms of both hardware and basic theory. In the area of the solid state especially, this period has seen the coming together of "chemical" and "physical" approaches to solids.[1−3] This period has witnessed some remarkable successes. The ability to study a wide range of complex materials using the tight-binding with overlap, or extended Hückel, approach has been well-established.[2] The success of tight-binding calculations to study complex systems by employing the technique of second moment conservation is an important advance.[4] Importantly, over this period there has been a transfer of tight-binding technology from the physical theorist to chemical theorist and in turn to the practicing solid-state chemist. In terms of numerically accurate methods, the ability from pseudopotential-based calculations to predict the transition pressure from one structure to another[5] and the prediction of properties such as hardness are milestones. The local density approximation[6] has provided for solids an effective way to estimate many-body effects. By using generalized gradient corrections (GGC), it has been possible with full potential LAPW calculations[7] to effectively probe the factors influencing the spin state of ions in solids or, more generally, the magnetic or localization behavior of electrons. (See ref 8 for a succinct description of the present state of this rapidly advancing field.) The LMTO method[9] is proving to be an extremely useful tool with which to study the electronic structure of solids, especially close-packed ones. (It is regarded by many hard-line theorists as an "old-fashioned" approach but has many advantages for the structural chemist.) Undoubtedly, the dramatic change in computational power over the past few years has accelerated the application of such methods to "real" systems. This has brought its problems, however. We now have even more numbers. The question of how to organize them and develop new insights and models of use to the chemist has certainly become a challenge.

In terms of the transfer of band-structure technology from physicist to chemist, quite striking is the often routine use of tight-binding theory[2] in its extended Hückel implementation by experimentalists. There are now an increasing number of papers

published (see for example refs 10−12) where this type of theoretical approach complements diffraction, magnetic, conductivity, and other physical methods in providing insights into the structure, both geometric and electronic, of a material. The role of the chemist in understanding the electronic structure of solids has for many years been "to add the atoms" and thus endeavor to view solids as individuals, rather than using the solid state physicists' often generic approaches using the ideas of quasiparticles. This particular role has been enhanced as the number of experimental solid-state chemists with a firm understanding of the band model increases. Such tight-binding calculations are computationally economical and often very revealing. In terms of quantitative results involving bond lengths and cohesive energies, they are not to be trusted (but see the discussion in section 5). The same caveats apply to their molecular analog, of course. In the right hands, the results have been used to provide extremely useful pictures of solid-state electronic structure.

Of particular interest in this direction is a recent development in the use of the electron localization function (ELF)[13] to explore bonding in solids. From a given set of occupied orbitals the method highlights those areas where paired electrons are most likely to be found. (We discuss this further in section 6.) The method apparently removes the arbitrariness often associated with the construction of localized functions from a delocalized one. The results seem virtually independent of the use of tight-binding, *ab initio*, or LMTO calculations as input. The challenge, as we have already noted, is to explore the real meaning behind the results and to try to build a picture of chemical bonding from the results. The ELF approach has real promise, and the development of global pictures from such calculations is a challenge for the future.

Numerically more accurate calculations are of two types: extensions of the *ab initio* method of the molecular chemist to solids and the use of physicists' approaches such as the LMTO and LAPW methods. In their full potential implementation which makes them as nearly *first principles* calculations as one can get (notice the difference between chemists' and physicists' terminology here), they can be very accurate in balancing one-electron and many-body terms in the energy. The extent of the utility of *ab initio* calculations in solids is presently being explored.[14] Just as there are problems with this approach in large molecules and in molecules where HOMO and LUMO are close in energy, so in solids the method has its limitations when dealing with metals. The next few years will see how useful the approach is in general to look at solids in a really
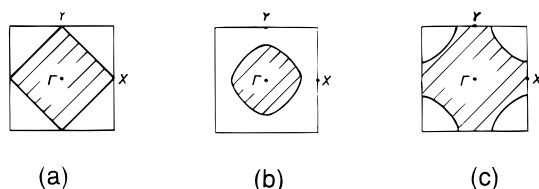
Figure 1. The Fermi surface for the square net of hydrogen atoms with (a) a half-filling of the energy band and (b, c) just under half and just over half-filling, respectively.

quantitative way. The problem with all of these many-electron models is their voracious appetite for computer time, a concern, of course, which may be alleviated with time. (History has shown, however, that we will always be demanding more from our calculations than we have in terms of computational resources.) This article shows how electronic structure calculations may be used to study a selected range of topics.

2. Fermi Surface and Charge Density Waves

One of the most important concepts in the area of solid-state structure is that of the Fermi surface.[15] It is of vital interest to the solid-state physicist interested in the transport properties of solids. The surface is the constant energy plot in **k** space of the highest occupied energy levels of the solid at $T = 0$. Put another way, it represents the junction between filled and empty levels. Obviously then, for a system where the energy bands are filled such that there is a gap between highest occupied and lowest unoccupied levels there is no Fermi surface at all, and thus the concept only applies to metals. The shape of the Fermi surface varies with electron count. Figure 1a shows the computed surface for a square net made up of hydrogen 1s orbitals. Figure 1b,c shows how the Fermi surface changes for the less-than-half-full and greater-than-half-full bands. All of these surfaces are described as being two-dimensional in character since they contain a closed loop. An open surface indicates a one-dimensional system. These two cases are experimentally readily distinguished, in principle at least.[16]

Particularly interesting are the predictions made when a section of the Fermi surface can be moved by a vector **q** so that it becomes superimposed on another section of the surface as in **1**. This is described as Fermi surface nesting, the two

1
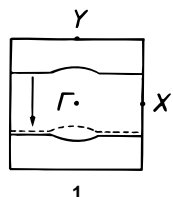
parts nested by the vector **q**. If large sections of the Fermi surface are nested, then this can lead to an electronically driven geometrical instability. The vector **q** defines the details of how the structure changes on distortion. For the simple one-dimensional case, if **q** = **b**/2 then a distortion which leads to a doubling of the unit cell in this direction is indicated. In general, if **q** = **b**/n then a distortion leading to a cell n times as large as the original one is predicted. This is just the classic Peierls distortion of the one-dimensional chain[2] (**2**). The hypothetical chain of equidistant hydrogen atoms with a half-filled band is an example where the Fermi surface is completely nested and $n = 2$. (In one dimension the Fermi surface is just a pair of points in the first Brillouin zone.) One can immediately see that the Peierls distortion has many features similar to those associated with the Jahn−Teller distortion in molecules. In **2** notice that a metal has been converted to an insulator as a result of the distortion.

2
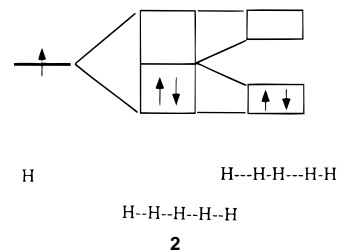
In more than one dimension some other considerations apply. The nesting of the Fermi surface may not be complete. For example, in Figure 1b,c the curvature of the Fermi surface which is generated by doping removes such nesting. In more complex systems only sections of the surface may be translated in this way. This means that the driving force for distortion is reduced and (as in the 1-D case too) has to compete with the elastic forces of the underlying structure which generally favor the undistorted structure. Frequently, although many states will be removed from around the Fermi level on distortion, a gap will not be opened up (as in **2**). As a result, although metallic, the distorted material is not quite as metallic as before. (TaS_2 is an example here.) Frequently there is a critical temperature below which the distortion, or charge density wave (CDW),[16,17] sets in. The distortion does not necessarily need to be commensurate with the lattice, and incommensurate charge density waves where n is not an integer are in fact frequently found. Diffuse X-ray scattering has been a particularly useful tool[18] with which to study these systems and identify **q**. Diffuse scatterings above a critical temperature develop into satellite reflections below this transition temperature, their spacings determined by **q**.

Particularly impressive over the past few years have been the prediction of the vector **q** from tight-binding calculations of the extended Hückel type by (especially) Canadell and Whangbo.[15] The systems which have been studied include metal oxides, particularly the bronzes, metal chalcogenides, and the molecular metals, the latter systems which contain largely organic molecules that are either intrinsically or extrinsically doped with electrons or holes (i.e., are either reduced or oxidized). We will discuss one example from the bronze area.

The molybdenum and tungsten oxides provide a wealth of interesting structural and electronic features.[19] The blue bronzes, $A_{0.3}MoO_3$ (A = K, Rb, Tl), are layered materials built up from $Mo_{10}O_{30}$ building blocks.[20] A metal-to-semiconductor transition occurs at around 180 K, and diffuse X-ray scattering shows that at room temperature $q \approx 0.72b*$ (an incommensurate distortion), where b is the crystallographic b axis. As the temperature is lowered, then **q** approaches[21] the commensurate value of $0.75b*$. A slice through the dispersion picture for this material[22] is shown in Figure 2. The Fermi level cuts the lowest two bands but only just misses the third highest (calculated energy separation 0.012 eV). Determination of **q** from the point where the Fermi level cuts the highest bands leads to $q = 0.75b*$. (This value is not obvious from the dispersion diagram of Figure 2. One has to study the complete Fermi surface, rather than a small part of it, as shown in Figure 2.) This is in exact agreement with experiment at low temperatures and tells us why the blue bronze undergoes a metal−semiconductor transition. (Calculating the temperature at which is occurs is more difficult. It depends upon the accurate assessment of the driving force associated with the electrons at the Fermi surface and the elastic forces of the deeper-lying ones.) The electronic structural details though are the key in understanding why there is a temperature dependence on **q**, an unusual result. Because of the low-lying third band, thermal depletion of the second band occurs as the temperature increases, thus changing its occupancy, lowering
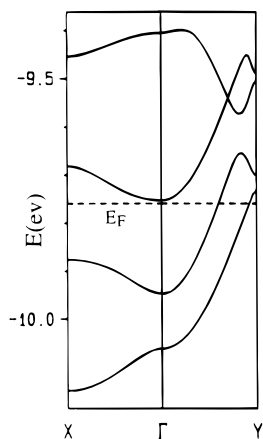
Figure 2. A part of the dispersion picture for the blue bronze A_xWO_3. The nesting vector itself has to come from the full Fermi surface. Adapted from ref 22.
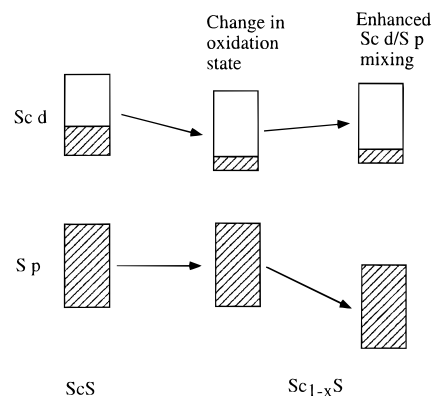

Figure 3. The mechanism for the stabilization of nonstoichiometric ScS.

Figure 4. Calculated density of states for ScS and of $Sc_{0.75}S$. Adapted from ref 28.

the Fermi level, and, as it turns out, moving **q** a smaller value along **b***. Tracing the origin of the band structure back to the details of the structure leads to an understanding of this process.[22]

Similar studies have been performed with molecular metals. Here, the tight-binding approach has come into its own. Not only are "better" calculations at present difficult to do for such extended systems, but the tight-binding approach gives excellent agreement with experiment. Future directions in this area will include surfaces, where Kohn anomalies (vibrational softening) have been well studied[23] for systems such as Mo, W(100). Here interest lies in the surface Fermi surface.

3. Stability of Solids

The general question of the stability of solids, identification of those which are "stable" and those which are not, is an exceedingly tough one to answer, since even for an AB solid, in principle all of the AB_{1-x} space needs to be examined energetically. This is at present an impossible task, and even study of a small part of the space is demanding in terms of computational time and theoretical rigor. Of course, one can always restrict the problem to comparison of the energies of a small subset of structures. Here we describe two studies which circumvent some of these problems, that of the origin of nonstoichiometry in ScS and the stabilization of high oxidation states of copper by generation of a ternary oxide containing an electropositive element.

Nonstoichiometry in rock salt oxides and chalcogenides is widespread,[24] but although the chalcogenides of the early transition metals form a variety of ordered and disordered phases extending to either side of the stoichiometric 1:1 composition, the fact that Sc leaves the solid on heating ScS rather than sulfur is somewhat surprising.[25] The cohesive energy of ScS is around 250 kcal/mol so that the solid itself is composed of strong bonds between the atoms. Chemists "explain" such a result by blandly stating that the Sc^{3+} generated by metal atom loss is "more stable" than the Sc^{2+} it replaces. But why? There have been early studies using the KKR method,[26] but a mechanism which leads to stabilization of metal vacancies was initially indicated from tight-binding calculations using self-consistent charge iteration and then verified using first principles LMTO calculations. The nub of the stabilization mechanism is shown in Figure 3.[27] Loss of metal but not of chalcogen leads to an increase in the oxidation state of the remaining metal atoms, $Sc^{2+} \rightarrow Sc^{3+}$. Since the levels at the very bottom of the metal d band are almost entirely metal in character in this system, they are expected to become more tightly bound as a result of
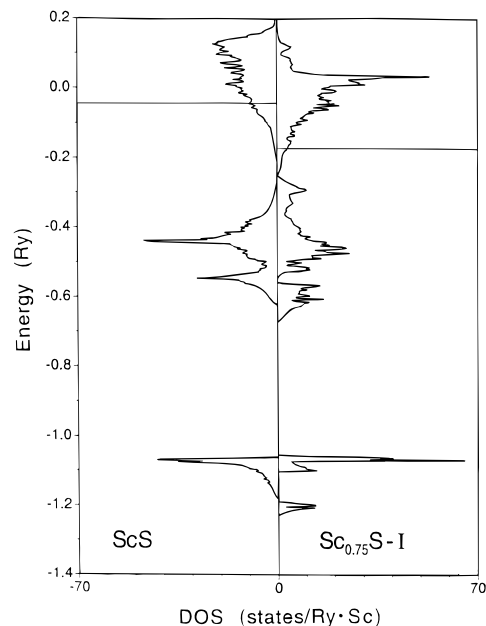
this change in oxidation state by simple analogy with the variation of atomic ionization energy with charge. Thus, the metal and chalcogen levels become closer in energy on loss of Sc, leading to an increase in their mutual interaction as metal is lost. The important result is stabilization of the filled, largely sulfur, levels. This leads to a stabilization associated with metal atom loss. Later transition metal chalcogenides such as FeS and MnS will not exhibit the same behavior since here the filled metal levels contain a significant amount of sulfur character, and their susceptibility to energetic change with metal oxidation state is smaller. The results from the numerically more accurate LMTO calculations[28] bear out these found from the charge-iterated tight-binding calculations.[27]

Figure 4 shows the computed electronic density of states for stoichiometric and defective ScS. The qualitative model described above may be reinforced in quantitative terms by calculation[28] of the mean energy of the (largely) sulfur 3p band by evaluating the expression $\sum n_i e(n_i)/\sum n_i$, where there are n_i states with an energy e_i. The results are found to be -0.4626, -0.4659, and -0.4758 Ry for ScS, $Sc_{0.875}S$, and $Sc_{0.75}S$, respectively, showing that in terms of lowering the energy of the sulfur 3p band the order is $Sc_{0.75}S > Sc_{0.875}S > ScS$, i.e., that there is indeed a driving force for loss of metal (1 Ry = 13.6 eV). They also show that Sc$-$S bonding becomes stronger when Sc is lost. The corresponding figures calculated for MnS and $Mn_{0.75}S$ are -0.5538 and -0.5499 Ry, respectively,

TABLE 1: Calculated Electron Populations and Band Barycenters (Ry) for Some Copper Oxides

| compd	$N_s{}^a$	N_p	N_d	N_{tot}	$C(M_s){}^b$	$C(M_p)$	$C(M_d)$	$C(O_p){}^c$
Cu_2O	0.546	0.464	9.340	10.350	−0.308	0.856	−0.286	−0.502
CuO	0.480	0.564	9.271	10.316	−0.327	0.833	−0.327	−0.410
Cu_2O_3	0.549	0.785	9.008	10.343	−0.436	0.721	−0.553	−0.507
								−0.453
$KCuO_2$	0.681	0.918	9.138	10.737	−0.504	0.644	−0.542	−0.446

^{a} N = number of electrons per copper. ^{b} C = energy barycenter of bands located on metal (M) and oxygen (O). ^{c} These two figures for Cu_2O_3 refer to the two different types of oxygen atom in the structure.

showing quantitatively that the strength of the Mn−S bonding in the stoichiometric compound is stronger than in the Mn-deficient one. This is in the opposite direction to the results for ScS and is in agreement with the lack of ready loss of metal from MnS and later metal chalcogenides. Notice that although the tight-binding model gave invaluable clues as to the electronic situation here, quantitative calculations which can be trusted in numerical terms are needed to firmly establish the mechanism. Such complementarity of the two types of calculation is invaluable.

A second example is the electronic model developed to understand the empirical observation[29] that high oxidation states of transition metals may often be stabilized as their oxide or nitride by the addition of an electropositive element. Thus, although copper is known as Cu(I) and Cu(II) in compounds with oxygen, no binary copper(III) oxide (Cu_2O_3) is presently known. Cu(III), however, may be stabilized as a ternary oxide as in $KCuO_2$. Similar observations are found for other oxides and nitrides. Bi(IV) is not found as a binary oxide, but $KBiO_3$ exists. Ce(IV) is not known as a binary nitride, but $BaCeN_2$ is a stable compound. Shown in Table 1 are the total number of $(n + 1)$s, $(n + 1)$p, and nd electrons calculated[30] using the LMTO method for Cu_2O, CuO, Cu_2O_3, and $KCuO_2$. Notice that contrary to the expectations of chemical intuition, of 10, 9, and 8 valence electrons for Cu(I), Cu(II), and Cu(III), respectively, we find 10.35, 10.32, and 10.74 electrons, a result which does not follow this trend. The d-electron populations do follow the expected decrease but with much smaller change than expected: 9.34, 9.27, and 9.14. The integral numbers of electrons used in our statement above assume the occupancy of "metal orbitals" which are 100% metal in character, and so these figures for the total number of "metal" electrons are a measure of the copper 4s, 4p, and 3d character which is mixed into the filled oxygen 2p band as a result of covalent interactions. The values for 4s and 4p in Table 1 indicate a large rehybridization at the metal atom (especially involving 4p) from one system to another. Since the metal 4s, 4p, and 3d levels change in energy with oxidation state, their interaction with the oxygen orbitals increases as their energy mismatch with oxygen 2p decreases.

Perhaps the most interesting comparison of the figures in Table 1 is that the total number of metal electrons, roughly equal in $Cu^I{}_2O$, $Cu^{II}O$, and $Cu^{III}{}_2O_3$, is much larger in $KCu^{III}O_2$. In other words, the bonds are computed to be much more covalent (actually in accord with early ideas[29] of Sleight) and thus presumably stronger in $KCuO_2$. This arises through this increase in metal 4s, 4p, and 3d involvement with the oxygen levels. It comes about because in $KCu^{III}O_2$ there is an effective transfer of charge from potassium to oxygen, leading to a raising of the oxygen levels, a decrease in the metal spd−oxygen 2p separation, and then, on energy gap arguments, the generation of a stronger interaction between copper and oxygen, i.e., an increase in Cu−O covalency. This interaction is particularly important for Cu(III), where the metal levels lie closest to those on oxygen.

This is a result which has a similarities to the electronic underpinnings[27,28] of the nonstoichiometry of ScS (to give
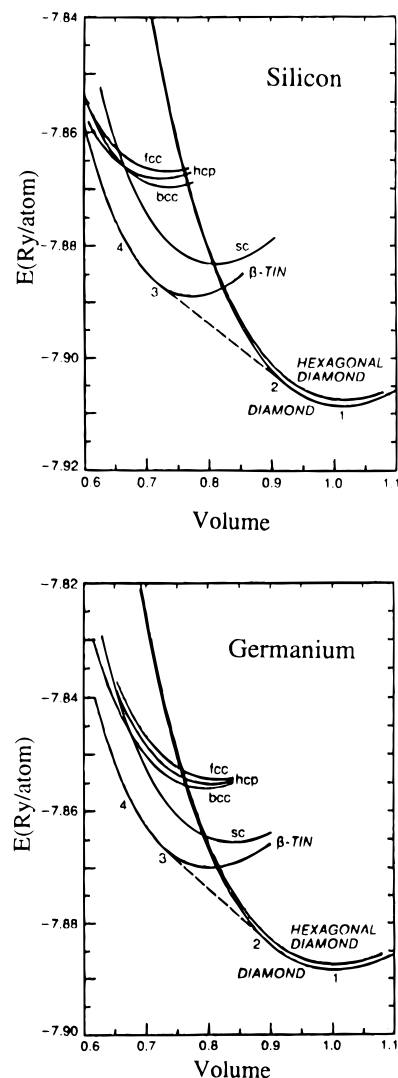

Figure 5. Calculated behavior under pressure of Si and Ge. Adapted from ref 31.

$Sc_{1−x}S$) described above. Both pairs of levels are driven closer to each other energetically either as the average oxidation state of the metal increases or as electron transfer to oxygen occurs.

4. Structures of Solids under Pressure

Of particular interest in providing clues as to the factors which influence the structures of solids and of great importance in the geophysical world is the behavior of solids under pressure. For several years the stage has been set by the pioneering work of Cohen and his collaborators. A view of the field in 1979 can be found in ref 5. Here the use of pseudopotential-based calculations was readily able to mimic experimentally observed structural changes and also give good agreement with the equation of state itself. Figure 5 shows the calculated[31] behavior under pressure of Si and Ge. A more recent example is the determination of the structure of elemental hydrogen under pressure, a result of interest to Jovian geophysicists. The initial report was a dramatic one. The calculated high-pressure structure, a metal, was calculated[32] to have an enormously high (over 200 K) critical superconducting transition temperature. A later study found[33] a slightly different structure to be more stable under pressure but with a much reduced T_c. These results highlight a problem with such studies. It is not possible to explore the entire geometrical space open to the structure, and so one is never sure that the structure found is the lowest energy one. Later studies may well find a lower energy variant.

Electronic Structure and Properties of Solids

J. Phys. Chem., Vol. 100, No. 31, 1996 **13267**
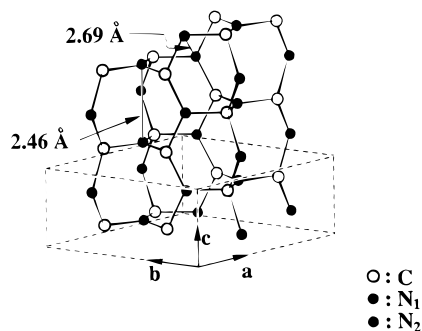
Figure 6. Structure of C_3N_4 (courtesy of T. Hughbanks).

Values for the compressibility of solids emerge naturally from such studies. It is interesting to note that it is harder experimentally to compress $Sc_{1-x}S$ than ScS, a result reproducible by calculation (M. T. Green, unpublished results). These results run contrary to the normal rule which associates higher compressibilities with smaller numbers of vacancies.

Another example, which has a moral associated with it, centers around the recent discussions concerning the prediction of hard materials. In an inventive theoretical paper Liu and Cohen, predicted[34] that the compound β-C_3N_4 if it had the known β-Si_3N_4 structure[35] would have a hardness comparable with or larger than that of diamond. In this structure (Figure 6) each carbon is coordinated by four nitrogen atoms, and correspondingly each nitrogen atom is three-coordinate. The equilibrium volume of β-C_3N_4 was determined by calculating the total crystal energy as a function of a single scale parameter.

This interesting theoretical result led to experimental efforts to make the new material. Carbon nitride films were made by reacting nitrogen atoms with gaseous carbon generated by laser ablation.[36] However, the largest percentage of nitrogen found in the films made in this way (45%) is much less than that expected for β-C_3N_4 (57%). Further work was not conclusive;[37] the nitrogen content of such films ranged from 0 to 50%, and there was some significant oxygen contamination ($\sim$5$-$10%).

The major problem with the theoretical study of β-C_3N_4 is that optimization of the cell volume alone gives no information as to whether the hypothetical structure will be stable with respect to $C_xN_y + zN_2$ (where $(y + z/2)/x = 4/3$). This is a consideration which we mentioned above. In the present case, however, there is quite a bit of structural information readily available which tells us that this structure is energetically unacceptable and should have been discarded early on. The nonbonded N$-$N contacts which are fine for the known silicon compound are much too short for the carbon analog using typical C$-$N bond distances and angles. The nonbonded repulsions which result between the nitrogen atoms will be strongly destabilizing. Theoretical estimates for the (large) energetic penalty in β-C_3N_4 from this source have been made, and a structurally related C_4N_3 alternative where such repulsions are avoided has been proposed.[38] Thus, getting behind the numbers from the calculation is an essential part of such theoretical studies. (Newer experimental work[39] shows that the nitrogen composition of C$-$N films saturates at less than 50% and that the predicted β-C_3N_4 remains at present experimentally inaccessible.)

5. Metal$-$Insulator Transitions

One of the most challenging areas in solid-state electronic structure theory is the identification of the factors which determine whether a material is a metal or an insulator. The field has been of interest for many years[40,41] but has received much more attention after the discovery of high-temperature superconductivity. One can delineate two broad categories of

metal$-$insulator transition which arise through two different electronic mechanisms. Mott$-$Hubbard insulators are systems where electrons are localized when the on-site electron$-$electron repulsion U is significantly larger than the bandwidth W. In other words, if there is an energy penalty for placing two electrons on the same atomic center, then electrons will not flow through the solid. Thus, the band gap arises through electron correlation. The second type of transition is one where the density of states is set by the geometry, so the gap between full and empty bands may be opened or closed by changing the structure. **3** shows the two mechanisms schematically using

3
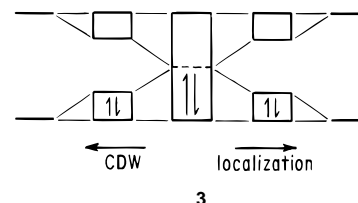
hydrogen as an example.[3] At large H$-$H distances (right) where U/W is large, the system is a Mott$-$Hubbard insulator. An insulator is also found when the H atoms form dimers at the far left. In the middle where the H$\cdots$H distances are equal but not large, the system is metallic. Many of the geometrical distortions of the second type include those described as Peierls or CDW distortions. The hydrogen example is representative of many geometrically and electronically more complex systems. Many metal$-$insulator transitions are triggered by changes in temperature. For example, VO_2 is a metal above 340 K where it adopts the undistorted rutile structure. Below this temperature the material is an insulator[42] with the MoO_2 structure, one where the metal atoms, which lie in chains, are paired up in a Peierls fashion. Often such metal$-$insulator transitions may be induced by application of pressure. Thus, hydrogen becomes metallic as noted in section 4.

Of course, it is possible that some metal$-$insulator transitions will be determined by effects of both types described above. Mott$-$Hubbard transitions are often associated with geometry changes, too. There is also the question of localization effects via disorder (Anderson localization[43]). Since many metal$-$insulator transitions are triggered by doping, e.g.,[44] $La_{2-x}Sr_xMnO_3$, all three mechanisms may play significant roles.

By and large it is a relatively simple matter to determine whether a given material is a metal or insulator controlled by effects of the second type. Calculations of the tight-binding type work well in showing the existence of gaps between filled and empty bands. The computed band gaps are usually too large using this method, but that is not usually a problem since this result is well-known and studies using the tight-binding approach are more often focused on qualitative pictures of the structure rather than on such numerical details. Band gaps using the LMTO method contrariwise are normally too small.

The real challenge in the area at present is the reliable computation of the energy of a metal relative to the Mott$-$Hubbard insulating state. This involves the introduction of electron correlation into the electronic structure problem.[3,40,41] In recent years density functional theory has made some dramatic contributions to the picture. With the aid of new density functionals which employ generalized gradient corrections,[45] energetic separation of metal and insulator is becoming increasingly accurate[6] using, for example, spin-polarized FLAPW calculation using the Perdew$-$Wang functional.[46] One can quite reliably predict that in the near future computational and theoretical advances will make this much more routine. Naturally, understanding how the gap originates is a much tougher assignment. It is associated with the proper inclusion of

correlation in the calculation, as noted earlier. In molecules the Møller−Plesset method[47] is frequently used, and the theoretical basis behind its structure enables ready evaluation of the quality of a particular calculation. With density functional theory it is not possible yet to decide whether one functional is better than another ahead of time. Another area, difficult from the viewpoint of electronic structure calculations, is the inclusion of disorder. Perhaps as larger systems become more readily approachable in computational terms, the results of large supercell calculations will lead to insights concerning this aspect of the metal−insulator question.

6. The Method of Moments

The geometrical structures of solids and the electronic factors which stabilize one polymorph over another are of great importance in solids, since the details of the structure often strongly influence the properties of the material. There are indeed many published band structure descriptions of solids, but an important question is whether there are any general statements which can be made that use a broader picture than the one where the structure and properties of each system are treated individually. The method of moments with its direct connection to the topology, or atomic connectivity of the solid, is a useful approach.[3,4,48,49] Recall that the *n*th moment of a collection of energy levels in terms of the electronic density of states, $\rho(E)$, is just $2\int_{-\infty}^{\infty}\rho(E)E^n \, dE$. It may be shown that within the Hückel model the *n*th moment may be written as a weighted sum over all the self-returning walks of the orbital problem as

$$\mu_n = \sum_{\text{walks of length } n} H_{ij}H_{jk}...H_{ni}$$

This result is shown pictorially in **4**. Note the direct connection between the moments and the geometrical structure.

4
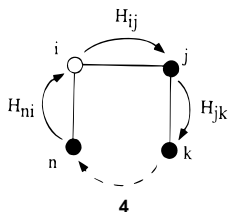
The first moment is just the sum of the "walks in place" and is thus a weighted sum of the diagonal terms of the Hamiltonian matrix, H_{ii} (α in Hückel language). It sets a "zero" of the energy scale. The second moment is an important parameter. It is the sum of the squares of the interaction integrals coupling one orbital (i) to its neighbors (j) as shown schematically in **5**. Thus, $\mu_2(i) = \sum_j H_{ij}H_{ji} = \sum H_{ij}^2$ and $\mu_2 = \sum_i \mu_2(i)$, where μ_2 is the second moment for the complete set of orbitals. Thus, the second moment is a good measure of the coordination strength around an atom.

5
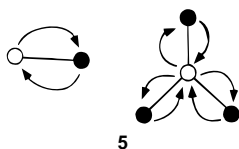
Higher moments describe how a given atom feels the presence of its neighbors further away. They give information about the electronegativity difference (difference in α values) between the atoms at each end of the bond and the presence of rings or loops in the structure (**6**, **7**). The fourth moment is another interesting parameter since it is the first in the CAB molecule

6

7
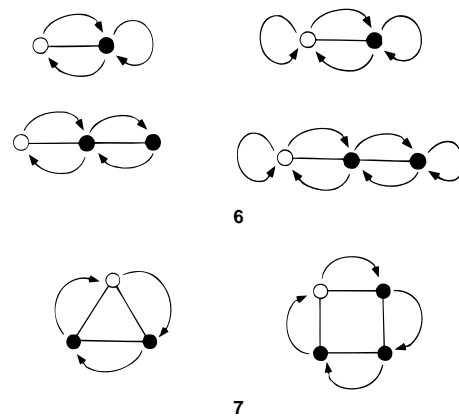
which allows atom B to "see" atom C via their chemical bonds to atom A.[50] Its magnitude depends on the CAB bond angle (H_{ij} depends on the angle) and so contains information about the shape of the system. Because the influence of an atom on its neighbors decreases as the distance between them increases, the importance of the higher moments drops off quickly as their order increases.

The second moment plays an important role in electronic−structural considerations. Although tight-binding calculations are notoriously inaccurate when it comes to comparing the stability of structures with different bond lengths or coordination numbers, reliable[2−4] energy differences (ΔE) between two structures may often be obtained by using the results of calculations performed using the Hückel ansatz $|\mathbf{H} - \mathbf{E}| = 0$ but setting the second moments of the energy density of states constant. (There is a simple argument for such second moment scaling from Lee[4] and Pettifor,[51] who call it the structural difference theorem.) As will be seen below, it is often useful to view ΔE as a function of electron count.

As described above, the second moment is determined by the number of neighbors around each atom and the values of the interorbital interaction integrals. Since these are determined by the interatomic separation, the second moment scaling scheme leads to insights into the way internuclear distances change with coordination number.[52] Although this may be shown for a simple orbital problem, it may be extended to more complex ones. For an atom with Γ neighbors and thus Γ interactions (which are assumed to be equivalent), then within the framework of Hückel theory $\mu_2 = \Gamma\beta^2 = q$, where q is a constant. Since the bond length (r) dependence of β may be generally written as $\beta = A/r^m$ in the region of chemical interest, the equilibrium interatomic separation is found to be $r_e^{2m} = \Gamma(A^2/q)$, namely an equilibrium bond length which increases with coordination number. This result may be tested. If a typical Si−O distance for four-coordinate silicon is 1.63 Å, then the value for six-coordinate silicon is predicted to be 1.80 Å (using $m = 2$), a figure in excellent agreement with experiment.

A considerably more complex example which relies on second moment conservation has led to the first viable explanation of the stability of the Hume-Rothery phases. Hume-Rothery realized[53] that the structures adopted by noble metal alloys, such as the brasses, are strongly determined by electron count. For many years they were called "electron compounds". The experimental data were for years interpreted using a model based on the nearly-free-electron model where the identity of the lowest energy structure changes when the Fermi surface moves through a Brillouin zone face.[54] Since the electronic structure of the transition metals and their crystal structures are well described[55] in terms of d-orbital interactions between adjacent atoms, it is not surprising that a similar orbital approach is successful for the five Hume-Rothery phases (hcp, bcc, fcc, β-Mn, and γ-brass), too. Figure 7 shows a comparison between

Electronic Structure and Properties of Solids

J. Phys. Chem., Vol. 100, No. 31, 1996 **13269**

Figure 7. Theoretically calculated and experimentally observed electron count ranges for stability of the Hume-Rothery phases. Adapted from ref 56.
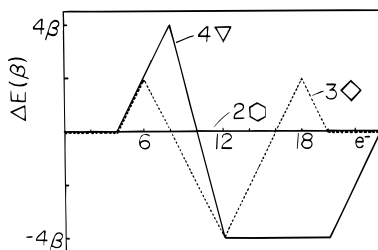

Figure 8. Energy difference between a two six-rings and p 12/p rings as a function of electron count. The fractional orbital occupancy is defined as (empty) $0 \leq x \leq 1$ (full). Adapted from ref 4.

identity of the lowest energy structure[56] from theory (using second moment conservation) and that found from experiment. Two of these structures, β-Mn and γ-brass, are very complex ones indeed. It is quite astonishing that the model correctly accommodates all of the different interatomic separations in a way that energetically resolves these structures as a function of electron count. In terms of the electronic densities of states of the solids involved,[3a] it is interesting to note that the more stable structure in each case is one that avoids high densities of states at the Fermi level and thus provides a connection with the traditional model.

The same approach[57] leads to good agreement between the experimentally and theoretically determined structures of binary alloys of the transition elements as a function of electron count. These structures include the very complex arrangements of the χ and σ phases. The agreement between theory and experiment is very good. It is difficult, however, to identify the structural features which stabilize one structure over another (see below). Note, however, that the stability of these two sets of compounds is simply determined by an (admittedly more complex) version of Hückel's rule, another "topological" theory.

Higher moments are important, too, and there is a general way to view the energy difference between two structures, $\Delta E(x)$, as a function of x, the band filling[48,49] (empty $0 \leq x \leq 1$; full) using them. Figure 8 shows results for the very simplest system. It shows energy differences as a function of electron count between rings of organic π systems of different sizes.[4] The results are in accord with Hückel's rule, but we can go further. Imagine two systems which have the same electronic densities of states. Then $\Delta E(x) = 0$. If the two densities of states differ first at the mth moment, then clearly it will be the properties of this mth moment (through the walks of **4**) which may be of major importance. There are two important features which will be useful in a global way.
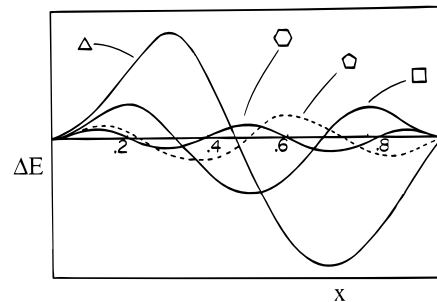

Figure 9. General $\Delta E(x)$ curves which represent the energetic difference between two systems whose densities of states differ at the nth moment indicated by an n-gon. The parameter x is the fractional orbital occupancy or band filling and is defined; empty, $0 < x < 1$, full. Adapted from ref 3. The dashed nature of one of the curves has no significance and is portrayed this way for clarity.

(a) The amplitude of the three curves of Figure 8 decrease in the order (12/p) = three rings > four rings. This trend is readily understandable in terms of the discussion above which identified structural walks as a measure of moments. When comparing a 12/p-membered ring with the six-membered ring, it is the first self-returning walk (moment) which will be different between the two which will dominate the form of $\Delta E(x)$. This will be the walk around the 12/p-membered ring of length 12/p (**7**). Therefore, in this new language the electronic situation for 12/p = 3,4 are third and fourth moment problems, respectively. This is the order of the first moment that is different between the two calculations.

(b) The number of nodes in these curves (including those at $x = 0$, 1) is equal to the order of the first disparate moment between the electronic densities of states of the two structures.[50] A set of $\Delta E(x)$ plots are shown in Figure 9. The structure which is more stable at the earliest orbital occupancy is[50] the one with the largest moment.

These two results lead to a direct correlation between the shape and amplitude of the energy difference curve, $\Delta E(x)$, between two structures and the geometries of the two structures. It is the way the atoms are connected together which determines the orbital walks which are possible and thus the orbital walks which are different between the two systems. There are some interesting generalities. Three-membered rings are most stable at early electron counts. The energy difference curves have a large amplitude for three-rings. Indeed, such structural features are commonplace in "electron-deficient" systems. Four-membered rings are associated with two regions of stability, at $x = 0.25$ and 0.75. Six-membered rings have three regions of stability, at $x = 0.167$, 0.5, and 0.833. In general terms at low electron counts (and especially at one-third filling), the three-rings are stable; at the half-filled point, six-membered rings are stable, and at higher electron counts (especially around three-quarters filling) four-rings are stable. The energy difference curves between the heavy elements on the right-hand side of the periodic table, Tl−Po, show these features.[50] Figure 10 shows calculated energy differences as a function of electron count (x for the p band) between the structures (simple cubic, hcp, ccp, and α-arsenic). Agreement with experiment is perfect. The early structures (lead and thallium) are dominated by three-rings (and thus close-packed structures), that at the half-filled point (bismuth) by the six-ring structure, and the squares which come in at later x for the simple cubic structure found for α-polonium. The simple form of the shapes of the curves determines which structure is stable at which electron count.

We are entering a stage where the execution of quite good theoretical calculations on solids is possible in a routine fashion. The discussion of this section underlines the importance of looking beyond the numbers and to the construction of
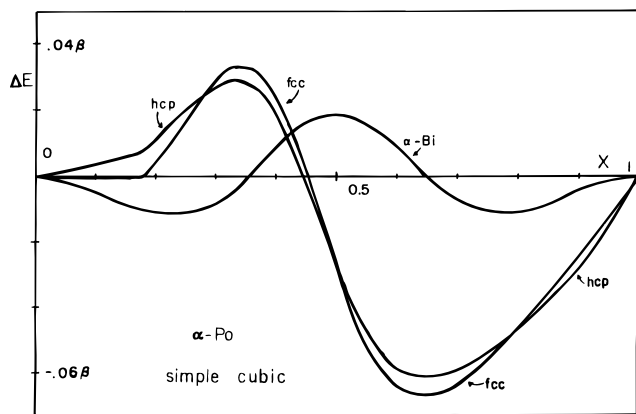
Figure 10. Computed energy difference curve as a function of band filling for the simple cubic, α-arsenic, hcp, and fcc structures. A p-orbital-only model was used. Notice the successful mimicking of the observed structures: Tl and Pb as close-packed structures with three-membered rings, Bi with the α-arsenic structure, and polonium with the simple cubic structure.

conceptually accessible electronic models. It is usually not easy. Recall Robert Mulliken's comment "the more accurate the calculations become, the more the concepts tend to vanish into thin air."[58] A useful model with much promise is described in the next section.

7. The Electron Localization Function

Almost since the time when chemists started to think about the topological connections between atoms which lead to molecules, they have also devised ways to view the chemical bond. Although we know that bonds exist (molecules do hold together), it has been very difficult to clearly correlate the bond with a measurable property of the molecule. Difference electron density maps, perhaps the obvious route, are not in general very helpful. The subtraction of atomic densities from the total electron density in a molecule does not take into account the rehybridization at each atom as it "prepares itself" for bonding. In some cases there is no difference density in a region where we know that there is a bond. We know too that the localization of electrons from delocalized molecular orbital pictures as often performed in molecules such as methane is perfectly arbitrary. For all collective properties of the molecule it does not matter which approach we use, a localized or delocalized one. This problem may have been solved by Becke and Edgecombe,[59] who introduced the idea of the electron localization function in 1990. It builds on an earlier idea of Lennard-Jones.[60] He used the two-particle density associated with electrons of parallel spin to study the spatial preferences of electrons. The two-particle density gives the joint probability function of finding one electron at (x,y,z) and another of the same spin at $(x',y'z')$. He found that electrons of parallel spin occupy separate regions of space, and thus one can imagine regions of paired electrons. The location of these localized electron pairs is not arbitrary, in contrast to the traditional ones derived from a molecular orbital picture.

Becke and Edgecombe[59] showed how the probability of finding two electrons with the same spin close together is very much dependent on location. They demonstrated how regions where the pair probability is high are regions where the electrons are poorly localized, but where the probability is low the electrons are well localized. ELF, the electron localization function, is actually numerically defined for a system with electron density $\rho(x,y,z)$ and set of occupied molecular orbitals $\{\phi_i\}$ as

$$\text{ELF} = 1/[1 + (D(x,y,z)/D_h(x,y,z))^2]$$

where

$$D(x,y,z)/D_h = 0.3483\rho^{-5/3}[\sum_i |\nabla\phi_i|^2 - \tfrac{1}{8}|\nabla\rho|^2/\rho]$$

D is the leading term in the expansion of the two-particle density in the interelectronic coordinate r_{12}, and the subscript h refers to the corresponding value for the homogeneous electron gas, the reference state. ELF as defined runs from 0 to 1 and is equal to 0.5 for the homogeneous electron gas.
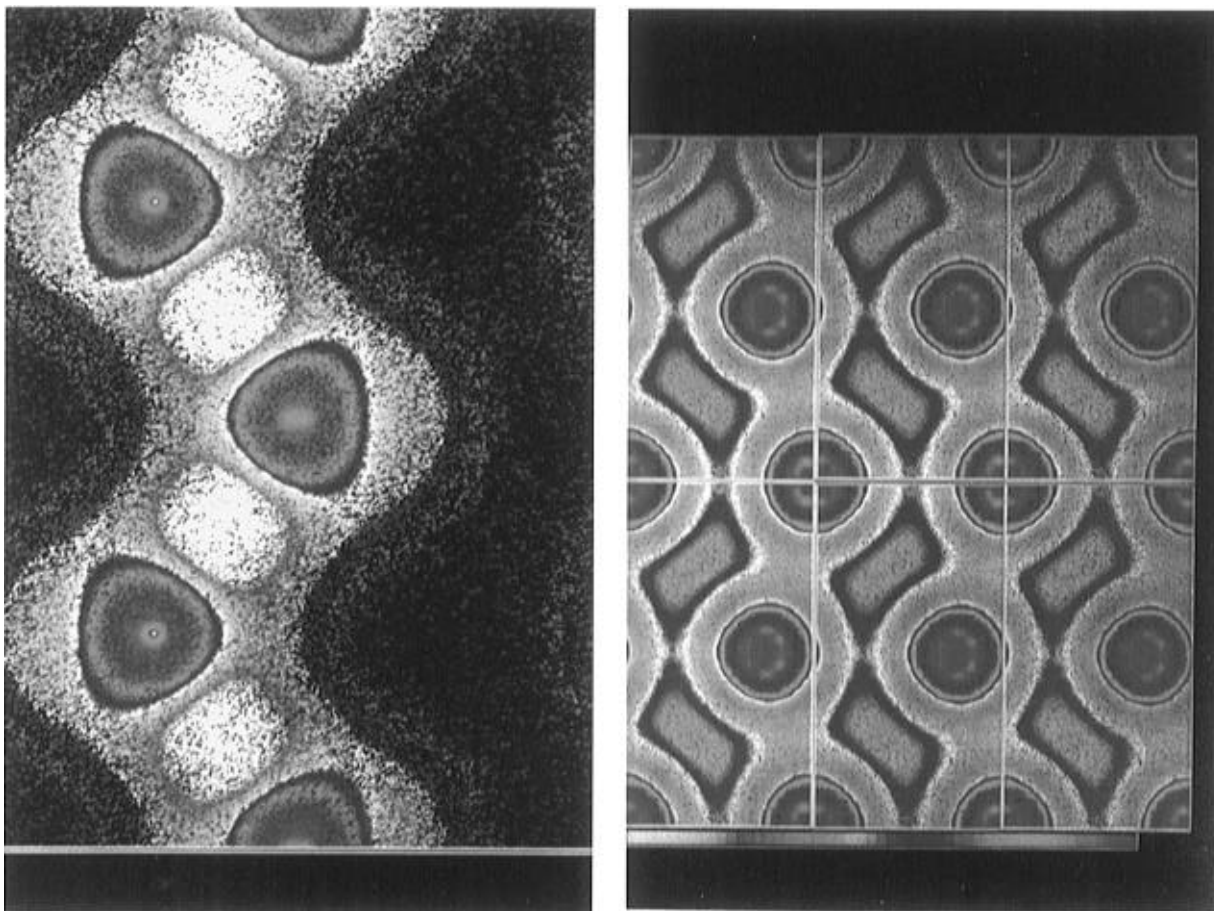
One can see a kinetic energy term ($|\nabla\phi_i|^2$) in this expression and can imagine that, if the kinetic energy is high, two electrons of the same spin will pass each other very quickly and thus that the wave function is highly localized. Conversely, a low local kinetic energy will indicate that the electrons are not highly localized. It turns out[13] that the results obtained by study of ELF pictures are usually independent of whether the wave functions and electron density have been generated using calculations which include electron−electron interactions (such as ab initio, LMTO, LAPW) or those which do not (Hückel and tight-binding calculations). This is in accord with the general ideas of chemical bonding. One-electron models have a long history in providing deep insights into fundamental aspects of structure and bonding. The essence of the picture may often be gained simply from orbital overlap and electrone-gativity considerations. The formal inclusion of electron−electron interactions usually only changes the bonding picture by a little. Figure 11 shows[61] some ELF maps for the elements C and β-Sn in the crystalline state. Just as in geographical maps the color code runs from blue (the oceans, low elevation, low ELF) through green, yellow, and brown to white (the mountains, high elevation, high ELF). In Figure 11a notice the regions of high localization (white) in the (110) plane, the C−C bonds in diamond. On moving down the periodic table there is a gradual decrease (not shown) in the extent of the white region and its replacement by brown regions showing regions of evenly distributed localization typical of the homogeneous electron gas. In Figure 11b for the metallic form of tin (β-Sn) there are no white regions and the localization (brown−yellow) only moderately high. These new results mesh with earlier views of this trend. On moving down the periodic table the valence s and p orbitals occupy increasingly disparate regions of space and the localized orbitals less localized. (See the discussion in ref 62.)

These ideas will certainly be of great importance in the future, and as we noted earlier a real challenge will be to develop new bonding models encompassing a wide range of solids, presently described from different viewpoints.

8. Superconductivity

The electronic structure and striking properties of the high-temperature superconductors have absorbed the attention of solid-state scientists for almost a decade since their discovery by Bednorz and Müller.[63] Even now we have very little understanding of what really sets these systems apart from other superconductors in terms of their electronic structure. (One interesting result of all of the attention, however, has been the exploration of copper oxide chemistry in a detail that is unprecedented in any other part of the periodic table.) The highest critical superconducting transition temperatures (T_c) are an order of magnitude larger than those previously known in conventional superconductors.[64] The highest T_c's found so far are around 125 K in the complex materials $Tl_2Ba_2Ca_2Cu_3O_{10}$, $TlBa_2Ca_3Cu_4O_{11}$, and $(Tl,Pb)Sr_2Ca_2Cu_3O_9$ and 153 K under pressure for $HgBa_2Ca_2Cu_3O_{8+\delta}$.

Electronic Structure and Properties of Solids

*J. Phys. Chem., Vol. 100, No. 31, 1996* **13271**

Figure 11. Computed ELF maps for (a, left) diamond in the (110) plane, a slice which shows the nearest-neighbor bonds, and (b, right) the metallic (β) form of tin. Reproduced by permission from ref 13b. Copyright 1994 Verlag Chemie.

A feature common to all of the superconducting cuprates[65] are sheets of stoichiometry CuO_2 (**8**) containing square-planar


8
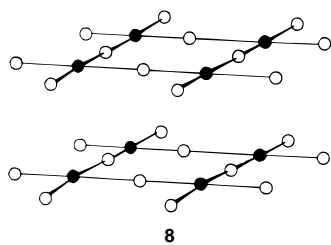
copper atoms. These sheets may be flat, puckered, or rumpled and frequently show one or two much longer Cu—O distances perpendicular to them. The copper oxidation state is always close to 2, and such local structures are those expected from Jahn—Teller considerations. These sheets, where superconduction takes place, alternate with sheets or slabs of, usually insulating but sometimes conducting, material. This is described as "reservoir" material as we will see below. It lies in a region spatially separated from the CuO_2 sheets (**9**). For example, in the "2—1—4 compound", $La_{2-x}Sr_xCuO_4$, written as $(La_{2-x}Sr_xO_2)(CuO_2)$ to emphasize its structure, the reservoir is a $La_{2-x}Sr_xO_2$ slab with the rock salt structure. In the "1—2—3 compound", $YBa_2Cu_3O_7$, $(Y)(Ba_2CuO_3)(CuO_2)_2$, there are two

9
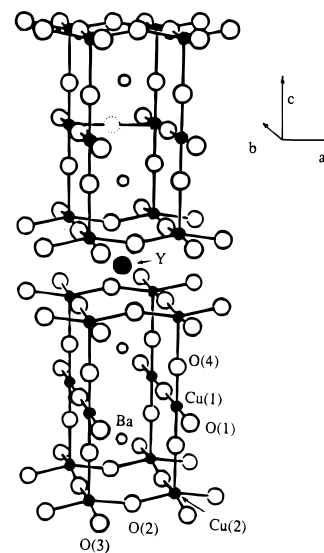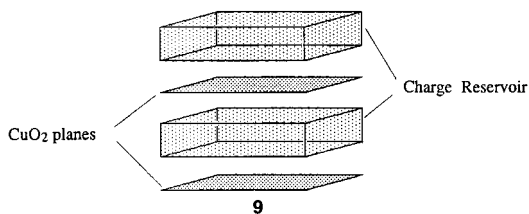
Figure 12. Structure of the 1—2—3 compound, $YBa_2Cu_3O_7$.

types of reservoir material (Figure 12): layers of Y atoms and the CuO_3 chains of square-planar Cu(2) linked by Ba atoms.

One feature common to all of these high-temperature superconductors is that[65] the copper oxidation state for the highest T_c is close to 2.15. Thus, for example, the maximum T_c in $La_{2-x}Sr_xCuO_4$ is for $x \approx 0.15$. Figure 13 shows a general picture which appears to be universal, although crystal chemistry often prohibits access to some doping regions in many systems. On initial doping of an antiferromagnetic insulator, the Néel temperature rapidly falls, and an ill-defined spin glass region appears to develop. At slightly higher doping levels a super-
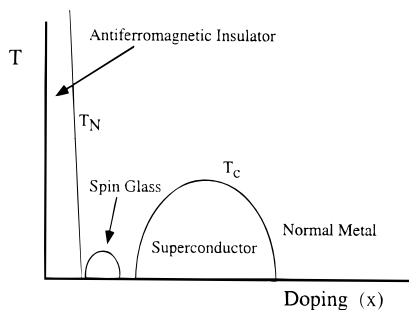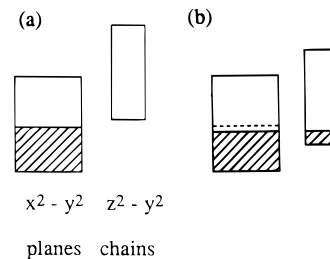
Figure 13. Schematic of the behavior of the $La_{2-x}Sr_xCuO_4$ compound with x. The nature of the material between insulator and superconductor is not clear.

Figure 14. The plane $x^2 - y^2$ band and chain $z^2 - y^2$ bands of YBa_2-Cu_3O_7. (a) An arrangement where no plane-chain electron transfer occurs. (b) Overlap of the two bands so that the chain copper atoms are reduced and the plane copper atoms oxidized.

conductor is produced with a maximum in T_c at this critical doping level. On further doping T_c drops, and a "normal" metal is produced. A second feature is that there appears to be a thermodynamic stabilization associated with this magic composition. Thus, on cooling La_2CuO_{4+x} below room temperature a phase separation[66] occurs into $La_2CuO_{4+x} \rightarrow La_2CuO_4 + La_2$-$CuO_{4.07}$. The second species has the magic electron count and is indeed a superconductor with a T_c similar to that in $La_{1.85}$-$Sr_{x.15}CuO_4$. In an extremely interesting study[67] of the series of oxides $Pb_2Sr_2RECu_3O_8$ (RE = rare earth), it was found that those examples with the larger REs (e.g., La) are semiconductors, but those with the smaller REs are superconductors with T_c's as high as 70 K. X-ray diffraction studies showed that the superconducting samples with, for example, RE = Ho contain around 9% vacancies on the RE site, whereas this site is fully occupied in the insulating examples. This figure of 9% RE vacancies for the superconductors leads to a value of 2.14 for the in-sheet copper oxidation state. There must be some feature of the chemistry which, during the synthetic step, drives the system to composition appropriate for the magic electron count.

Although there has been some progress,[68] one of the challenges for the future in this area is to identify the electronic features behind these observations, namely the origin of the thermodynamic driving force for the magic composition and its connection with a rather special type of superconductivity. Correlation with superconductivity will need to await suitable progress in solid-state physics.[69]

In three of the examples we have noted above, the magic copper oxidation state is achieved by varying the stoichiometry of the reservoir region, $(La_{2-x}Sr_xO_2)$ in $La_{2-x}Sr_xCuO_4$, (La_2O_{2+x}) in $La_2CuO_{4.07}$, and $(Pb_2Sr_2RECuO_4)$ in $Pb_2Sr_2RECu_3O_8$. A rather different and very interesting state of affairs (self-doping) is found in the 1−2−3 compound[70] $YBa_2Cu_3O_7$, with a T_c of ~95 K. This material (Figure 12) contains two types of copper atom: square-pyramidal Cu(1) and square-planar Cu(2). The fifth Cu(1)−O distance is quite long, so that a good description of the structure is of chains of copper (Cu(2)) in square-planar coordination sandwiched between planes of copper (Cu(1)). (Oxygen is readily lost from the chains, and copper atoms in linear two coordination are generated. In $YBa_2Cu_3O_6$ all of the interplanar copper atoms are two coordinate.) Since square-planar coordination is a feature of the structural chemistry of both Cu(II) and Cu(III) but the square-pyramidal arrangement, with a long apical bonds, only for Cu(II), $YBa_2(Cu^{II}O_2)_2(Cu^{III}O_3)$ should be a chemically satisfying way to describe $YBa_2Cu_3O_7$. In a similar way, $YBa_2(Cu^{II}O_2)_2(Cu^IO_2)$ should describe YBa_2-Cu_3O_6, since linear two-coordination is a common coordination geometry for Cu(I). Such simple descriptions clearly tell us little about the real state of affairs in the superconductor, and we need to examine the form of the band structure of the material.

This is shown in Figure 14 in schematic form and immediately shows a more complex picture. The $x^2 - y^2$ band

derived from the square planes is of δ symmetry with respect to the interplanar material and is thus essentially electronically decoupled from the energy bands of the chains. For the square-planar copper atoms of the chains an analogous $x^2 - y^2$ band may be constructed, labeled $z^2 - y^2$ since these chains run in the yz plane. The actual electronic description of this compound critically depends on the relative locations of these two bands as may be seen from Figure 14. These two bands actually overlap in such a way that electron transfer occurs[71,72] from plane to chain (Figure 14b). As a result, the interplanar CuO_3 unit plays the same role as substitution of Sr for La in the La_2-CuO_4 system, the overall result being removal of electron density from the CuO_2 planes. The geometrical details of the copper coordination are vital in controlling this charge transfer since the Cu−O distances in particular set the widths and centers of the bands. Such band overlap is found in other superconductors[73] such as $Tl_2Ba_2Ca_{n-1}Cu_nO_{2n+4}$.

As we have noted above, a clear challenge for the future is the elucidation of the nature of the electronic state in these solids. All of the presently known high-T_c superconductors may be described using the schematic of Figure 13, which shows how the superconductor evolves from the antiferromagnetic insulating state through an ill-defined spin-glass state on doping. Eventually a normal metal is generated at high doping levels. We noted earlier that metal−insulator transitions may be controlled by correlation (Mott−Hubbard transitions), changes in geometry dictated by Fermi surface nesting, and localization effects via disorder. In the superconductors where a wide doping range has been available for study (e.g., for $La_{2-x}Sr_xCuO_4$ itself), the geometry generally changes rather smoothly with x even though the space group may change. The elucidation of the nature of the metal−insulator or superconductor−insulator transition in this system is a particularly demanding challenge and is associated with the construction of a mechanism for superconductivity. From electronic structure calculations it is clear, however, that the copper "$x^2 - y^2$" band of the CuO_2 sheet is in fact heavily mixed with oxygen character and that this mixing is quite sensitive to the copper oxidation state. By analogy with results from lower temperature superconductors, there have been some interesting correlations from calculation[74] between the optimal doping level and the coincidence of the Fermi level with a van Hove singularity.

The important electronic features behind the superconducting properties of the alkali-metal-doped C_{60} solids[75,76] of stoichiometry A_3C_{60} are readily accessible. The highest T_c is currently 40 K. Many of these A_3C_{60} solids are described by a cubic close-packed array of C_{60} fullerene molecules with the A atoms in all the octahedral and tetrahedral holes. Others are based on a bcc arrangement. Recalling the stability of $C_5H_5{}^-$, high electron affinities for the attachment of electrons to C_{60} might be expected from the presence of the five-membered rings in this spherical polyene, and indeed, from the Hückel level structure of the system[76] (**10**), six electrons may be accom-

Electronic Structure and Properties of Solids

*J. Phys. Chem., Vol. 100, No. 31, 1996* **13273**
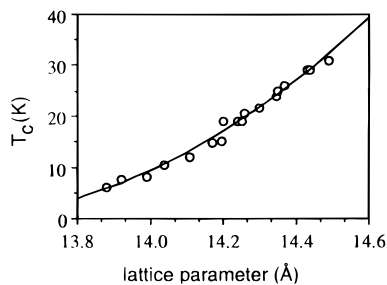
Figure 15. Dependence of T_c on cell parameter for fullerene-based A_3C_{60} solids. The different points correspond to different metals A and/or different pressures. Adapted from ref 2b.

Figure 16. Dependence of ln T_c on calculated density of states at the Fermi level ($\rho(E_F)$) for fullerene-based A_3C_{60} solids. The data points are selected from those in Figure 15. Adapted from reference 2b.

modated to give an semiconductor by filling the t_{1u} band. (The degeneracies of the levels are shown on the right-hand side of the diagram. With three electrons, however, the half-filled band for A_3C_{60} leads to a metal and superconductor.
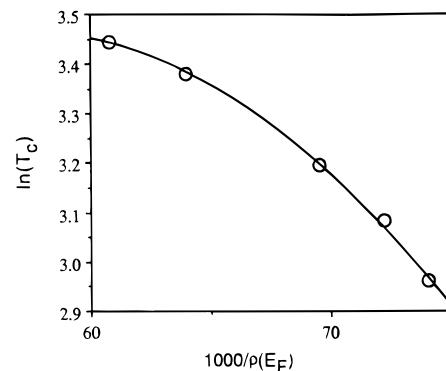

10
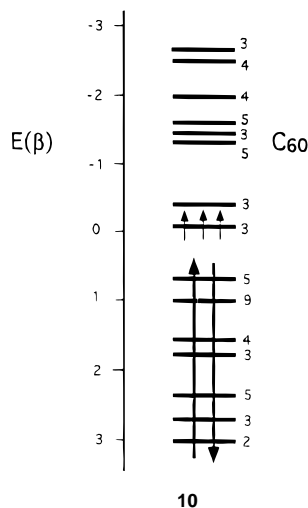
The dependence[75] of T_c upon cell parameter in a variety of doped fullerenes is shown in Figure 15. This behavior has a simple explanation based on the structural dependence of the band structure using the BCS formulation of superconductivity. This formally envisages the generation of a Cooper pair via an attractive potential, V, which exists within the range of phonon energies E_D around the Fermi energy, namely $E_F \pm E_D$. Within the phonon scheme E_D is just $k\theta_D$ where T_c is the Debye temperature. T_c is given by $1.134\theta_D \exp(-1/V\rho(E_F))$, where θ_D is the Debye frequency, $V\rho(E_F)$ is a dimensionless term, the electron−phonon coupling constant. $\rho(E_F)$ is the density of states at the Fermi level. As the size of the dopant increases, the fullerene units are pushed further apart with a concomitant decrease in the overlap integral between adjacent molecules. This overlap integral determines the bandwidth; the larger the overlap integral, the larger the bandwidth (**11**) and thus the
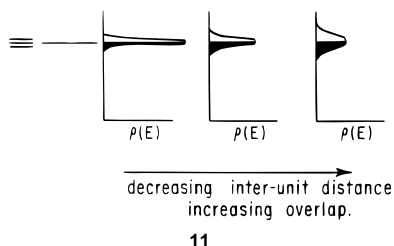
11

smaller the density of states at the half-filled point (since the total integrated density of states is constant). Assuming that θ and V of the BCS equation are invariant to the nature of metal atom substitution, then T_c varies simply with $\rho(E_F)$ as shown

by calculation in Figure 16. Higher T_c's are found for larger intermolecular C−C distances where the overlap is smaller. At some limiting separation, however, the bandwidth will have decreased to the point where the delocalized model becomes inappropriate and the electrons localize. The effect destroys not only superconductivity but normal metallic behavior, too. This has probably occurred for $(NH_3)_6Na_3C_{60}$[77] where the Na-$(NH_3)_2$ unit, larger than a naked Na^+ ion, leads to a large interunit C−C separation. Again, a challenge for calculation is to be able to reproduce (and predict in for other cases) the occurrence of these transitions by balancing the one-electron and many-body terms in the energy.

9. Epilogue

In this article we have reported on some diverse types of solid-state problems using an equally wide range of theoretical methods. What is interesting is how theoretical methods, often quite sophisticated, are becoming increasingly used by the experimental chemist as a tool along with physical instrumental methods. Thus, the group of users of theory is larger that the group of "theorists", a welcome state of affairs. The use of theory in any area of science requires a knowledge, not only of its implementation but also of its limitations of course. It also demands, to be effective, the ability to step back from the numbers generated by the computer and construct a theoretical model which will be useful, not only for the system at hand but also for a much broader spectrum of materials. Although some of the theoretical problems facing us are described in the text above, the generation of global pictures of the electronic structure of solids remains our greatest challenge. At present, given the stoichiometry of a $A_xB_yC_z$ solid, we cannot in general predict its structure, let alone its properties. This venture transcends advances which will be made in the future in terms of computational power and improvements in the numerical accuracy of our theoretical methods. This is where the real excitement will lie.

References and Notes

(1) See, for example: *Bonding and Structure of Solids*; Haydock, R., Inglesfield, J. E., Pendry, J. B., Eds.; The Royal Society of London: London, 1991.

(2) (a) Hoffmann, R. *Solids and Surfaces*; VCH Publishers: Cambridge, 1988. (b) Burdett, J. K. *Chemical Bonding in Solids*; Oxford: 1995.

(3) (a) Pettifor, D. G. *Bonding and Structures of Molecules and Solids*; Oxford: New York, 1995. (b) Sutton, A. P. *Electronic Structure of Materials*; Oxford: New York, 1993.

(4) Lee, S. *Acc. Chem Res.* **1991**, *24*, 249.

(5) See the impressive state of the art in 1979 in: Cohen, M. L. *Phys. Today* **1979**, *32*, 40.

(6) Labanowski, J. K.; Andzelm, J. W. *Density Functional Methods in Chemistry*; Springer-Verlag: New York, 1991.

(7) Wimmer, E.; Krakauer, H.; Weinert, M.; Freeman, A. J. *Phys. Rev.* **1983**, *B24*, 864.

(8) Dufek, P.; Blaha, P.; Sliwko, V.; Schwarz, K. *Phys Rev* **1994**, *B49*, 10170.

(9) Andersen, O. K. *Phys. Rev.* **1975**, *B12*, 3060. Skriver, H. L. *The LMTO Method*; Springer-Verlag: Berlin, 1984, and references therein. Andersen, O. K.; Skriver, H. L.; Nohl, H. *Pure Appl. Chem.* **1979**, *52*, 93.

(10) Nesper, R. *Angew. Chem., Int. Ed. Engl.* **1991**, *30,* 789.

(11) Miller, G. J.; Li, F.; Franzen, H. F. *J. Am. Chem. Soc.* **1993**, *115*, 3733.

(12) Guloy, A. M.; Corbett, J. D. *Inorg. Chem.* **1993**, *32*, 3540.

(13) (a) Savin, A.; Becke, A. D.; Flad, J.; Nesper, R.; Preuss, H.; von Schnering, H. G. *Angew. Chem.*, *Int. Ed. Engl.* **1991**, *30*, 409. (b) Hässermann, U.; Wengert, S.; Hofmann, P.; Savin, A.; Jepson, O.; Nesper, R. *Angew. Chem., Int. Ed. Engl.* **1994**, *33*, 2069.

(14) Pisani, C.; Dovesi, R.; Roetti, C. *Hartree-Fock Ab Initio Treatment of Crystalline Systems*; Springer-Verlag: Berlin, 1988.

(15) Canadell, E.; Whangbo, M.-H. *Chem. Rev.* **1991**, *91*, 965.

(16) Wilson, J. A.; DiSalvo, F. J.; Mahajan, S. *Adv. Phys.* **1975**, *24*, 117.

(17) Pouget, J. P.; Comes, R. In *Charge Density Waves in Solids*; Gor'kov, L. P., Grüner, G., Eds.; Elsevier: Amsterdam, 1989.

(18) E.g.: Kobayashi, H.; Kobayashi, A. In *Extended Linear Chain Compounds*; Miller, J. S., Ed.; Plenum Press: New York, 1982; Vol. 2.

(19) *Low-Dimensional Properties of Molybdenum Bronzes and Oxides*; Schlenker, C., Ed.; Kluwer: Dordrecht, The Netherlands, 1989. See the different reviews in the special issue of *Int. J. Mod. Phys.* **1993**, *B7*, 3937−4164.

(20) Graham, J.; Wadsley, A. D. *Acta Crystallogr.* **1966**, *20*, 93.

(21) Pouget, J. P.; Kagoshima, S.; Schlenker, C.; Marcus, J. *J. Phys. Lett.* **1983**, *44*, L113.

(22) Whangbo, M.-H.; Schneemeyer, L. F. *Inorg. Chem.* **1986**, *25*, 2424.

(23) Smith, K. E.; Kevan, S. D. *Phys. Rev.* **1991**, *B43*, 1831, 3986. Di, W.; Smith, K. E.; Kevan, S. D. *Phys. Rev.* **1991**, *B43*, 12062.

(24) Sørensen, O. T., Ed. *Nonstoichiometric Oxides*; Academic Press: New York, 1981. Kosuge, K. *Chemistry of Nonstoichiometric Compounds*; Oxford University Press: London, 1994.

(25) Burdett, J. K.; Mitchell, J. F. *Prog. Solid State Chem.* **1995**, *23*, 131.

(26) Misemer, D. K.; Nakahara, J. F. *J. Chem. Phys.* **1984**, *80*, 1964. Teunge, R. T.; Laabs, F.; Franzen, H. F. *J. Chem. Phys.* **1976**, *65*, 2400. Franzen, H. F.; Nakahara, J. F.; Misemer, D. K. *J. Solid State Chem.* **1986**, *61*, 338.

(27) Burdett, J. K.; Mitchell, J. F. *Chem. Mater.* **1993**, *5*, 1465.

(28) Burdett, J. K.; Sevov, S.; Mryasov, O. *J. Phys. Chem.* **1995**, *99*, 2696.

(29) Sleight, A. W. In *Chemistry of High-Temperature Superconductors*; Vanderah, T. A., Ed.; Noyes: Park Ridge, NJ, 1991. Sleight, A. W. *Science (Washington, D.C.)* **1988**, *242*, 1519.

(30) Burdett, J. K.; Sevov, S. *J. Am. Chem. Soc.* **1995**, *117*, 12788.

(31) Yin, M. T.; Cohen, M. L. *Phys. Rev.* **1982**, *B26*, 5668.

(32) Barbee, T. W. III; Cohen, M. L. *Phys. Rev.* **1991**, *B43*, 5269.

(33) Barbee, T. W. III; Cohen, M. L. *Phys. Rev.* **1991**, *B44*, 11563.

(34) Liu, A. Y.; Cohen, M. L. *Science (Washington, D.C.)* **1989**, *245*, 841.

(35) Hardie, D.; Jack, K. H. *Nature* **1957**, *180*, 332.

(36) Niu, C.; Lu, Y. Z.; Lieber, C. M. *Science (Washington, D.C.)* **1993**, *261*, 334.

(37) Yu, K. M.; Cohen, M. L.; Haller, E. E.; Hansen, W. L.; Liu, A. Y.; Wu, I. C. *Phys. Rev.* **1994**, *B49*, 5034.

(38) Hughbanks, T.; Tian, Y. *Solid State Commun.* **1995**, *96*, 321.

(39) Zhang, Z. J.; Fan, S.; Lieber, C. M. *Appl. Phys. Lett.* **1995**, *66*, 3582.

(40) Mott, N. F. *Metal-Insulator Transitions*; Taylor and Francis: London, 1974.

(41) (a) Goodenough, J. B. *Magnetism and the Chemical Bond*; Wiley: New York, 1963. (b) Goodenough, J. B. *Prog. Solid State Chem.* **1971**, *5*, 143. (c) Cox, P. A. *The Electronic Structure and Chemistry of Solids*; Oxford: London, 1987.

(42) Anderson, G. *Acta Chem. Scand.* **1956**, *10*, 623.

(43) Anderson, P. W. *Phys. Rev.* **1958**, *109*, 1492.

(44) Møller, C.; Plesset, M. S. *Phys. Rev.* **1936**, *46*, 618. Pople, J. A.; Binkley, J. S.; Seeger, R. *Int. J. Quantum Chem.* **1976**, *S10*, 1.

(45) E.g.: Cox, P. A. In Cheetham, A. K., Day, P., Eds. *Solid State Chemistry: Compounds*, Oxford: London, 1992.

(46) Perdew, J. P. In *Electronic Structure of Solids '91*; Ziesche, P., Eschrig, H., Eds.; Akademie-Verlag, 1991.

(47) Perdew, J. P.; Chevary, J. A.; Vosko, S. H.; Jackson, K. A.; Pederson, M. R.; Singh, D. J.; Fiolhais, C. *Phys. Rev.* **1992**, *44B*, 6671.

(48) Burdett, J. K. *Struct. Bonding (Berlin)* **1987**, *65*, 30.

(49) Burdett, J. K. *Acc. Chem. Res.* **1988**, *21*, 189.

(50) Burdett, J. K.; Lee, S. *J. Am. Chem. Soc.* **1985**, *107*, 3063.

(51) Pettifor, D. G.; Podloucky, R. *J. Phys. (Paris)* **1986**, *C19*, 285.

(52) Burdett, J. K.; Hawthorne, F. C. *Am. Mineral.* **1993**, *78*, 884.

(53) Hume-Rothery, W. *The Metallic State*; Oxford: London, 1931.

(54) Jones, H. *The Theory of Brillouin Zones and Electronic States in Crystals*, 2nd ed.; North-Holland: Amsterdam, 1975.

(55) Pettifor, D. G. *J. Phys. (Paris)* **1970**, *C3*, 367. Pettifor, D. G. *Calphad.* **1977**, *1*, 305.

(56) Lee, S.; Rousseau, R.; Wells, C. *Phys. Rev.* **1992**, *B46*, 12121. Hoistad, L. M.; Lee, S.; Pasternak, J. *J. Am. Chem. Soc.* **1992**, *114*, 4790.

(57) Hoistad, L. M.; Lee, S. *J. Am. Chem. Soc.* **1991**, *113*, 8216.

(58) Mulliken, R. S. *J. Chem. Phys.* **1965**, *43*, S2.

(59) Becke, A. D.; Edgecombe, K. E. *J. Chem. Phys.* **1990**, *92*, 5397.

(60) Lennard-Jones, J. E. *J. Chem. Phys.* **1952**, *20*, 1024.

(61) Savin, A.; Becke, A. D.; Flad, J.; Andersen, O. K.; Preuss, H.; von Schnering, H. G. *Angew. Chem., Int. Ed. Engl.* **1992**, *31*, 187.

(62) Kutzelnigg, W. *Angew. Chem., Int. Ed. Engl.* **1984**, *23*, 272.

(63) Bednorz, J. G.; Müller, K. A. *Z. Phys.* **1986**, *B64*, 189. Müller, K. A.; Bednorz, J. G. *Science (Washington, D.C.)* **1987**, *237*, 1133.

(64) Cava, R. J. *Science (Washington, D.C.)* **1990**, *247*, 656. Rao, C. N. R.; Raveau, B. *Acc. Chem. Res.* **1989**, *22*, 106. Sleight, A. W. *Science (Washington, D.C.)* **1988**, *242*, 1519. Vanderah, T. A., Ed. *Chemistry of High-Temperature Superconductors*; Noyes: Park Ridge, NJ, 1991. Williams, J. M.; Beno, M. A.; Carlson, K. D.; Geiser, U.; Kao, H. C. I.; Kini, A. M.; Porter, L. C.; Schultz, A. J.; Thorn, R. J.; Wang, H. H. *Acc. Chem. Res.* **1988**, *21*, 1.

(65) Burdett, J. K. *Adv. Chem. Phys.* **1993**, *83*, 207.

(66) Jorgensen, J. D.; Dabrowski, B.; Pei, S.; Hinks, D. G.; Soderholm, L.; Morosin, B.; Schirber, J. E.; Venturini, E. L.; Ginley, D. S. *Phys. Rev.* **1988**, *B38*, 11337. Jorgensen, J. D.; Dabrowski, B.; Richards, D. R.; Hinks, D. G. *Phys. Rev.* **1989**, *B40*, 2187.

(67) Xue, J. S.; Reedyk, M.; Greedan J. E.; Timusk, T. *J. Solid State Chem.* **1993**, *102*, 492. Xue, J. S.; Greedan J. E.; Maric, M. *J. Solid State Chem.* **1993**, *102*, 501.

(68) Burdett, J. K. *Acc. Chem. Res.* **1995**, *28*, 227.

(69) Emery, V. J.; Kivelson, S. A. *Physica C* **1993**, *209*, 597.

(70) Hor, P. H.; Meng, R. L.; Wang, Y. Q.; Gao, L.; Huanh, Z. J.; Bechtold. J.; Forster, K.; Chu, C. W. *Phys. Rev. Lett.* **1987**, *58*, 1891.

(71) Burdett, J. K.; Kulkarni, G. V. *Phys. Rev.* **1989**, *B40*, 8908.

(72) Yu, J.; Massidda, S.; Freeman, A. J.; Koelling, D. D. *Phys. Lett.* **1987**, *A122*, 283.

(73) Jung, D.; Whangbo, M.-H.; Herron, N.; Torardi, C. C. *Physica* **1989**, *C160*, 381.

(74) Norman, M. R.; McMullan, G. J.; Novikov, D. L.; Freeman, A. J. *Phys. Rev.* **1993**, *B48*, 9935.

(75) Fischer, J. E.; Heiney, P. A.; Smith, A. B. *Acc. Chem. Res.* **1992**, *25*, 112.

(76) Haddon. R. C. *Acc. Chem. Res.* **1992**, *25*, 127.

(77) Henry, P. F.; Rosseinsky, M. J.; Watt, C. J. *Chem. Commun.* **1995**, 2131.